DOI: https://doi.org/10.68732/e0d1584d31f07f20

ISBN: 978-9989-2053-6-1

Estimation of boundary stresses of high-pressure lined rock caverns using superposition of Inglis solutions

L. Uotinen, M.A. Aydoğmuş & M. Janiszewski
Aalto University, Espoo, Finland
lauri.uotinen@aalto.fi
0000-0001-9646-5029

Abstract

Lined rock caverns (LRCs) are a promising solution for high-pressure hydrogen storage in crystalline bedrock, where early-stage design requires rapid assessment of geometry-dependent boundary stresses. Existing approaches are either analytically rigorous but impractical for scoping, or flexible but computationally expensive.

This study presents a linear-elastic approximation for estimating boundary stresses in ellipsoidal caverns by superimposing classical Inglis solutions and applying a geometric reprojection to approximate three-dimensional effects. Internal pressure is incorporated through FEM calibrated stress intensity factors.

The method is evaluated against three-dimensional finite element models over a wide range of aspect ratios and stress conditions representative of Finnish bedrock. For far-field loading, the approach reproduces numerical results with typical errors of 2-5 MPa. For pressurised cases, the inclusion of stress intensity factors improves agreement, reducing errors to below 1 MPa for roof stresses and 0.5-1 MPa for wall stresses.

The results indicate that far-field stress redistribution can be approximated reasonably using reprojected two-dimensional solutions, whereas pressure-induced stresses require curvature-dependent correction. The proposed method provides a fast tool for early-stage design and parametric screening, while identifying conditions where full numerical modelling remains necessary.

Keywords

Boundary stresses, Kirsch solution, Inglis solution, LRC, Superposition, Hydrogen storage.

1 Introduction

Lined rock caverns (LRCs) are a viable option for large-scale high-pressure (e.g., 20 MPa internal pressure) hydrogen storage in crystalline bedrock, particularly in regions without salt formations such as Finland. At the energy system level, underground storage is required to buffer variability in renewable energy production. A Finnish case study identified LRCs as the most cost-efficient option under such conditions (Pekkinen et al., 2026). Following system-level feasibility, the key question becomes how cavern geometry influences boundary stresses.

Previous studies on LRC mechanics, analytical solutions for elliptical openings, and experimental investigations consistently highlight the strong influence of geometry, loading conditions, and internal pressure on stress distribution and stability (Damasceno et al., 2023; Masoudi et al., 2024; Leong et al., 2025; Patel & Desai, 2020; Zhao et al., 2021).This problem is grounded in classical elasticity. For three-dimensional ellipsoidal openings, Lukić et al. (2009) derived convergent series solutions, while Chiang (2015) demonstrated systematic dependence of stress concentration on shape ratios and the non-trivial link between two- and three-dimensional behaviour. Yin et al. (2022) further showed sensitivity to loading and boundary conditions. Together, these studies confirm that boundary stresses in ellipsoidal openings are strongly geometry-dependent and cannot be reliably inferred from simplified two-dimensional analogies.

At the applied level, numerical studies show that depth, aspect ratio, and internal pressure jointly control whether stresses remain compressive or become tensile. Uotinen and Rinne (2025) showed that unpressurised caverns favour oblate geometries, whereas pressurised caverns shift towards prolate forms, with tensile stresses increasing rapidly at insufficient depth. This highlights a gap between exact three-dimensional solutions, which are rigorous but cumbersome, and numerical modelling, which is flexible but computationally intensive. In early-stage design, this gap limits exploration of large parameter spaces. Analytical approximations, if sufficiently accurate, enable near-instant evaluation and systematic parameter sweeps, offering speedups of 1000x – 10 000x compared to numerical modelling.

Classical solutions such as Kirsch and Inglis provide useful benchmarks but do not extend directly to finite three-dimensional caverns. This study addresses the gap by estimating boundary stresses in ellipsoidal openings through superposition of Inglis-type solutions aligned with the principal axes, with the third stress component obtained from equilibrium with internal pressure. The approximation is exact at the principal-axis intersections and approximate elsewhere, and its accuracy is evaluated against three-dimensional numerical models under stress conditions representative of Finnish crystalline bedrock.

2 Methods

In this paper two analysis methods are used: numerical modelling using the finite element method using Comsol Multiphysics 6.4 software to approximate the boundary stresses around ellipsoid openings and superposition of analytical 2D solutions to construct an approximation of the stress state. For both analysis cases, the shape of the cavern is approximated with an ellipsoid with subradii $r_x$along X-axis, r_y along y-axis, and $r_z$along Z-axis (Fig. 1). The X-axis is oriented along the major in-plane stress σ_H, Y-axis along the minor horizontal stress σ_h, and the Z-axis along the vertical stress σ_V.

The method assumes linear elasticity, homogeneity, and isotropy. The superposition is exact only at principal-axis intersections and approximate elsewhere. The reprojection and pressure correction factors are empirically fitted over a limited height to width aspect ratio range of 1:5 to 5:1. Pressure effects are not derived analytically and are therefore less rigorous than far-field stress estimates.

2.1 Initial data

For the purposes of testing, typical values for material parameters in Finland (Table 1) and a typical coastal stress state (Table 2) at a depth of zmeters from the Olkiluoto island in Finland are used.

Table 1. Material parameters.

Parameter		Value
density [kg/m^3]	ρ	2700
Young's modulus [GPa]	E	40
Poisson's ratio [1]	ν	0.25

Table 2. Stress field.

Parameter		Value
vertical stress [MPa]	σ_V	0.26487 · z
major horizontal stress [MPa]	σ_H	13.0 + 0.031 · z
minor horizontal stress [MPa]	σ_h	8.5 + 0.024 · z

2.2 Classical 2D solutions

Classical linear-elastic solutions provide the baseline for estimating stress concentrations around underground openings. The Kirsch (1898) solution describes stresses around a circular hole in an infinite plate and shows that tangential stress at the boundary varies with angle, reaching a maximum of three times the far-field stress under uniaxial loading. The Inglis (1913) solution extends this to elliptical openings with horizontal subradii r_x and vertical subradii r_z, introducing explicit dependence on aspect ratio (r_z/r_x) and demonstrating that stress concentration increases with elongation,

approaching crack-like behaviour for highly prolate geometries. These solutions establish that boundary stresses are strongly geometry-controlled even under simple loading. Table 3 shows the solutions for the tangential stress in the roof and wall for both formulas as a function of the horizontal stress (σ_h) and the vertical stress (σ_v).

However, both Kirsch and Inglis formulations are inherently two-dimensional and assume an infinite elastic medium with uniform far-field stress. They do not account for variation along the cavern axis, finite length effects, or general three-dimensional stress states, and there is no direct closed-form extension to arbitrary ellipsoidal cavities suitable for design use. Consequently, while these solutions are valuable for benchmarking and rapid scoping, their direct applicability to finite three-dimensional caverns is limited.

Table 3. Boundary stresses for roof and wall using the analytical solutions.

Tangential stress at	Kirsch 1898	Inglis 1913
roof	$\sigma_{roof,K} = 3\sigma_h - \sigma_v$	$\sigma_{roof,I} = \sigma_h\left(1 + 2\frac{r_z}{r_x}\right) - \sigma_v$
wall	$\sigma_{wall,K} = 3\sigma_v - \sigma_h$	$\sigma_{wall,I} = \sigma_v\left(1 + 2\frac{r_x}{r_z}\right) - \sigma_h$

For the tangential stress resulting from the internal pressure, we can use the formulas 1 and 2

roof
$$\sigma_{\vartheta\vartheta} = \sigma_{xx} = -p_{int}\left(2\frac{r_z}{r_x} - 1\right) \quad (1)$$

wall
$$\sigma_{\vartheta\vartheta} = \sigma_{zz} = -p_{int}\left(2\frac{r_x}{r_z} - 1\right) \quad (2)$$

Assuming plane-strain ($\varepsilon_{yy} = 0$), for the change in out-of-plane (Y) stresses we can use the formulas

roof
$$\Delta\sigma_{yy} = \nu[(\sigma_{xx} + \sigma_{zz}) - (\sigma_H + \sigma_V)], \sigma_{zz} = p_{int} \quad (3)$$

wall
$$\Delta\sigma_{yy} = \sigma_H\nu[(\sigma_{xx} + \sigma_{zz}) - (\sigma_H + \sigma_V)], \sigma_{xx} = p_{int} \quad (4)$$

2.3 Geometric conversion from 2D to 3D

A geometric conversion of the stress trajectories must be made to convert from a true cylinder (an ellipse with infinitely long aspect ratio) to a circle (1:1 aspect ratio). The trial function was selected so that at 0 it will result the original stress state (=0) and at infinity it will result in the Kirsch 2D solution (=1). The shape exponent (1.166) was fitted over the aspect ratio range from 1:5 to 5:1 height to width. The approximate formula is then:

$$\omega\left(r_i/r_j\right) = \frac{\left(r_i/r_j\right)^{1.166}}{1 + \left(r_i/r_i\right)^{1.166}} \wedge i, j \in x, y, z \quad (5)$$

2.4 Reprojected Kirsch

A geometric reprojection of the stress trajectories can be made to convert from a true cylinder (an ellipse with infinitely long aspect ratio) to a circle (1:1 aspect ratio). The approximate formulae are:

roof
$$\sigma_{xx} = \sigma_H + 2\sigma_H\omega\left(r_y/r_z\right) - \sigma_V\omega\left(r_y/r_x\right) \quad (6)$$

roof
$$\sigma_{yy} = \sigma_h + 2\sigma_h\omega\left(r_x/r_z\right) - \sigma_V\omega\left(r_y/r_x\right) \quad (7)$$

wall (X)
$$\sigma_{zz} = \sigma_V + 2\sigma_V\omega\left(r_y/r_x\right) - \sigma_H\omega\left(r_y/r_z\right) \quad (8)$$

wall (X)
$$\sigma_{yy} = \sigma_h + 2\sigma_h\omega\left(r_y/r_x\right) - \sigma_H\omega\left(r_y/r_z\right) \quad (9)$$

2.5 Reprojected Inglis

A geometric reprojection of the stress trajectories can be made to convert from a true cylinder (an ellipse with infinitely long aspect ratio) to a circle (1:1 aspect ratio). The approximate formulae are:

roof
$$\sigma_{xx} = \sigma_H + 2\left(r_z/r_x\right)\sigma_H\omega\left(r_y/r_z\right) - \sigma_V\omega\left(r_y/r_x\right) \quad (10)$$

roof
$$\sigma_{yy} = \sigma_h + 2\left(r_z/r_y\right)\sigma_h\omega\left(r_x/r_z\right) - \sigma_V\omega\left(r_y/r_x\right) \quad (11)$$

wall (X) $$\sigma_{zz} = \sigma_V + 2\left({}^{r_x}/_{r_z}\right)\sigma_V\omega\left({}^{r_y}/_{r_x}\right) - \sigma_H\omega\left({}^{r_y}/_{r_z}\right) \quad (12)$$

wall (X) $$\sigma_{yy} = \sigma_h + 2\left({}^{r_y}/_{r_z}\right)\sigma_h\omega\left({}^{r_y}/_{r_x}\right) - \sigma_H\omega\left({}^{r_y}/_{r_z}\right) \quad (13)$$

2.6 Internal pressure stress intensity factor

For the boundary stresses induced by the internal pressure in 3D ellipsoids, no geometrical conversion applies. Instead, a stress intensity factor must be defined as a function of the aspect ratio. The correction factors were fitted over the aspect ratio range from 1:5 to 5:1 height to width:

roof $$\sigma_{\vartheta\vartheta} = \sigma_{xx} = \sigma_{yy} = -\frac{p_{int}}{2}K_{roof}\left({}^{r_i}/_{r_j}\right) \quad (14)$$

wall $$\sigma_{\vartheta\vartheta} = \sigma_{xx} = \sigma_{yy} = -\frac{p_{int}}{2}K_{wall}\left({}^{r_i}/_{r_j}\right) \quad (15)$$

and the stress intensity factor estimates are

roof $$K_{roof}\left({}^{r_i}/_{r_j}\right) = 1 + 1.2626ln\left({}^{r_i}/_{r_j}\right) - 0.07162\left[ln\left({}^{r_i}/_{r_j}\right)\right]^2 - 0.11414\left[ln\left({}^{r_i}/_{r_j}\right)\right]^3 \quad (16)$$

wall $$K_{wall}\left({}^{r_i}/_{r_j}\right) = 1 + 1.8134ln\left({}^{r_i}/_{r_j}\right) - 0.29796\left[ln\left({}^{r_i}/_{r_j}\right)\right]^2 - 0.04647\left[ln\left({}^{r_i}/_{r_j}\right)\right]^3 \quad (17)$$

3 Results

Several tests were conducted to compare the FEM and the superposition approach. The sanity checks were done without internal pressure for an ellipsoid with circular shape in XZ and YZ planes. Later, a series of aspect ratios ranging from 1:5 to 5:1 height-to-width were compared with FEM solutions.

3.1 Verification against 2D solutions

As a baseline, the analytical implementation was first verified against classical Kirsch and Inglis solutions in limiting two-dimensional cases. The results calculated at centroid of ellipsoid at z = -100 m ($\sigma_H = 16.1$ MPa, $\sigma_h = 10.9$ MPa, $\sigma_V = 2.6$ MPa) are for Kirsch and Inglis:

Table 4. In XZ-plane (along major stressσ_H).

Tangential stress at	Kirsch 1898	Inglis 1913	FEM
roof (σ_{xx})	45.7 MPa	45.7 MPa	45.6 MPa
roof (σ_{yy}, Eq. 3)	17.7 MPa (10.9 + 6.8)	17.7 MPa (10.9 + 6.8)	17.6 MPa
wall X (σ_{zz})	-8.3 MPa	-8.3 MPa	-8.3 MPa
wall X (σ_{yy}, Eq. 4)	4.2 MPa (10.9 - 6.7)	4.2 MPa (10.9 - 6.7)	4.2 MPa

Table 5. In YZ-plane (along minor stressσ_h).

Tangential stress at	Kirsch 1898	Inglis 1913	FEM
roof (σ_{yy})	30.1 MPa	30.1 MPa	30.1 MPa
roof (σ_{xx}, Eq. 3)	20.3 MPa (16.1 + 4.2)	20.3 MPa (16.1 + 4.2)	20.2 MPa
wall Y (σ_{zz})	-3.1 MPa	-3.1 MPa	-3.1 MPa
wall Y (σ_{xx}, Eq. 4)	11.9 MPa (16.1 – 4.2)	11.9 MPa (16.1 – 4.2)	12.0 MPa

Table 6. In XZ-plane (along minor stressσ_h), with internal pressure of $p_{int} = 20$ MPa.

Tangential stress at	Kirsch 1898	Inglis 1913	FEM
roof (σ_{xx})	25.7 MPa	25.7 MPa	45.6 MPa
roof (σ_{yy})	17.7 MPa	17.7 MPa	17.6 MPa
wall X (σ_{zz})	-28.3 MPa	-28.3 MPa	-8.3 MPa
wall X (σ_{yy})	4.2 MPa	4.2 MPa	4.2 MPa

3.2 Spherical cavity

For a spherical cavity without internal pressure, the reprojected analytical solution provides a close approximation of the FEM results (Table 7). At the roof, the analytical stresses of 30.9 MPa and 20.5 MPa compare well with FEM values of 31.7 MPa and 21.6 MPa, corresponding to errors of approximately 3-5%. At the wall, the analytical estimates also remain within 10 % of the numerical results. This indicates that the superposition and reprojection approach captures the three-dimensional redistribution of far-field stresses accurately for symmetric geometries.

When internal pressure of 20 MPa is introduced, the agreement remains acceptable for the spherical case. The analytical solution predicts roof stresses of 20.9 MPa and 10.5 MPa compared to FEM values of 21.7 MPa and 11.6 MPa, corresponding to errors of approximately 4-10% (Table 8). At the wall, the agreement is similarly good for the dominant stress component, although deviations increase for the secondary component.

Table 7. Spherical cavity, with internal pressure of $p_{int} = 0$ MPa.

Tangential stress at	Reprojected Kirsch Eqs. 6-9	Reprojected Inglis Eqs. 10-13	FEM
roof (σ_{xx})	30.9 MPa (-3 %)	30.9MPa (-3 %)	31.7 MPa
roof (σ_{yy})	20.5 MPa (-5 %)	20.5 MPa (-5 %)	21.6 MPa
wall X (σ_{zz})	-2.9 MPa (-7 %)	-2.9 MPa (-7 %)	-3.5 MPa
wall X (σ_{yy})	13.8 MPa (+9 %)	13.8 MPa (+9 %)	12.7 MPa

Table 8. Spherical cavity, with internal pressure of $p_{int} = 20$ MPa.

Tangential stress at	Reprojected Kirsch Eqs. 6-9	Reprojected Inglis Eqs. 10-13	FEM
roof (σ_{xx})	20.9 MPa (-4 %)	20.9 MPa (-4 %)	21.7 MPa
roof (σ_{yy})	10.5 MPa (-10 %)	10.5 MPa (-10 %)	11.6 MPa
wall X (σ_{zz})	-12.9 MPa (-4 %)	-12.9 MPa (-4 %)	-13.5 MPa
wall X (σ_{yy})	3.8 MPa (+35 %)	3.8 MPa (+35 %)	2.8 MPa

3.3 Ellipsoid caverns

For no internal pressure ($p_{int} = 0$ MPa, Eqs. 10 & 12), the fits reproduce the overall trend but with a systematic bias. Roof stresses are captured within 2-4 MPa (max. 5 MPa), while wall stresses show 1-3 MPa deviations, with larger relative errors near the zero-crossing due to small magnitudes (Fig. 1).

For internal pressure of $p_{int} = 20$ MPa (Eqs. 10+14& 12+15),the agreement is good. Roof stresses are typically within 1 MPa of the FEM results, and wall stresses within 0.5-1 MPa. Relative errors are generally below 5-10%, except at large aspect ratios where stresses approach zero (Fig. 2).

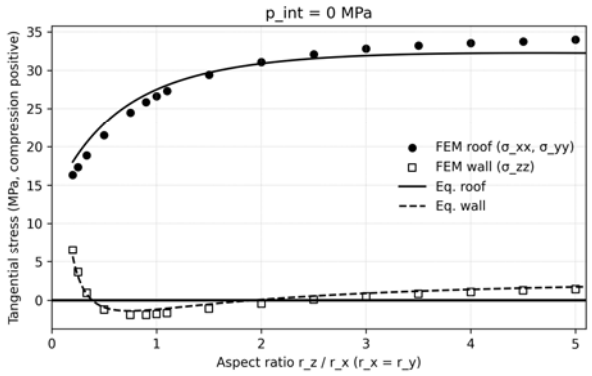


Figure 1. Solutions for unpressurized ellipsoid caverns.

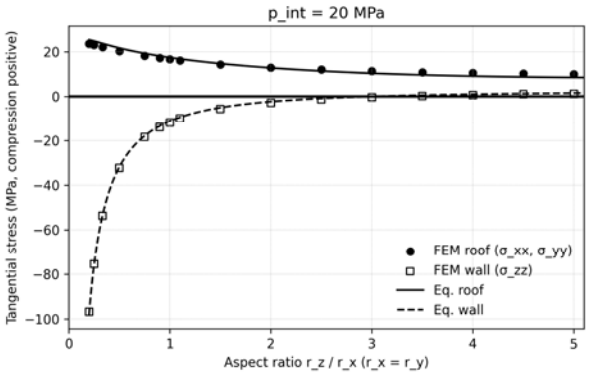


Figure 2. Solutions for ellipsoid caverns with 20 MPa internal pressure.

4 Discussion

The method is suitable for rapid scoping of far-field effects. For pressurised caverns, it captures trends but requires calibrated factors or numerical modelling for design. Superposition of Inglis-type solutions with geometric reprojection provides a consistent approximation for boundary stresses under far-field loading. For spherical and moderately elongated geometries, the method reproduces FEM results with acceptable accuracy, indicating that three-dimensional stress redistribution can be approximated by reweighting two-dimensional solutions.

For internal pressure, the behaviour deviates from this framework. While a simple scaling holds for spherical cavities, it does not extend to ellipsoids. The method overestimates tensile stresses at the roof and underestimates redistribution at the walls, with errors increasing with aspect ratio. This reflects a fundamental difference: far-field stresses redistribute through the rock mass, whereas internal pressure acts as a boundary traction governed by local curvature. As a result, pressure-induced stresses are not captured by superposition alone and require correction using stress intensity factors.

5 Conclusion

Superposition of Inglis-type solutions with geometric reprojection provides a simple and computationally efficient method for estimating boundary stresses in ellipsoidal caverns under far-field loading. The approach yields acceptable accuracy for spherical and moderately elongated geometries and is well suited for rapid scoping and parametric studies. Internal pressure cannot be represented within the same framework, as it is governed by local curvature rather than stress redistribution in the rock mass. Consequently, pressurised cases require calibrated correction factors or numerical modelling for reliable design.

Acknowledgments

This work was inspired by the main outcomes from the HUG (Hydrogen UnderGround research project 2024-2026) and earlier contract research work with a company that wishes to remain unnamed. During the preparation of this work, the authors used ChatGPT to check the language and improve readability. After using AI, the authors reviewed and edited the content as needed and take full responsibility for the content of the publication.

References

Chiang, C.-R. (2015). Stress concentration around a triaxial ellipsoidal cavity in transversely isotropic materials. Archive of Applied Mechanics, 85, 469-479. https://doi.org/10.1007/s00419-014-0923-1

Damasceno, D. R., Spross, J., & Johansson, F. (2023). Rock mass response for lined rock caverns subjected to high internal gas pressure. J. Rock Mech. Geotech. Eng., 15(1), 119–129. https://doi.org/10.1016/j.jrmge.2022.03.006

Inglis, C. E. (1913). Stresses in a plate due to the presence of cracks and sharp corners. *Transactions of the Institution of Naval Architects*, *55*, 219–241.

Kirsch, G. (1898). Die Theorie der Elastizität und die Bedürfnisse der Festigkeitslehre. *Zeitschrift des Vereins Deutscher Ingenieure*, *42*, 797–807.

Leong, C. M., Ghayesh, M. H., Nathan, G. J., Salmachi, A., & Rajabi, M. (2025). A review of the mechanics of lined engineered cavities and their implications on hydrogen storage. Int. J. Hydrogen Energy, 102, 749–766. https://doi.org/10.1016/j.ijhydene.2024.12.467

Lukić, D., Prokić, A., & Anagnosti, P. (2009). Stress-strain field around elliptic cavities in elastic continuum. European Journal of Mechanics - A/Solids, 28(1), 86-93. https://doi.org/10.1016/j.euromechsol.2008.04.005

Masoudi, M., Hassanpouryouzband, A., Hellevang, H., & Haszeldine, R. S. (2024). Lined rock caverns: A hydrogen storage solution. J. Energy Storage, 84, 110927. https://doi.org/10.1016/j.est.2024.110927

Patel, A., & Desai, C. K. (2020). Stress concentration around an elliptical hole in a large rectangular plate subjected to linearly varying in-plane loading on two opposite edges. Theor. Appl. Fract. Mech., 106, 102432. https://doi.org/10.1016/j.tafmec.2019.102432

Pekkinen, S., Muoniovaara, M., Seppälä, E., Pirhonen, P., Rinne, M., & Santasalo-Aarnio, A. (2026). Hydrogen storage model for decarbonization of constant industrial processes. Next Energy, 10, 100484. https://doi.org/10.1016/j.nxener.2025.100484

Uotinen, L., & Rinne, M. (2025). Rock mechanical optimization of the shape and depth for a high-pressure lined rock cavern. In Proceedings of the ISRM International Symposium Eurock 2025 - Expanding the Underground Space, Trondheim, Norway, 16-20 June 2025. https://airdrive.eventsair.com/eventsairwesteuprod/production-atlanticmice-public/5d50a02b6a3643d2a152c555202eb7b5

Yin, J., Liao, H., Kong, L., Cheng, J., Niu, T., Wang, X., & Zhuang, P. (2022). Analytical solution for elastic analysis around an ellipse with displacement-controlled boundary. Mathematical Problems in Engineering, 2022, Article 2148947. https://doi.org/10.1155/2022/2148947

Zhao, H., Sun, H., Zhang, D., & Liu, C. (2021). Mechanical properties and progressive failure characteristics of sandstone containing elliptical and square openings subjected to biaxial stress. PLOS ONE, 16(3), e0246815. https://doi.org/10.1371/journal.pone.0246815